Journal of Physics and Chemistry of Solids 171 (2022) 110995

Contents lists available at ScienceDirect

Journal of Physics and Chemistry of Solids

journal homepage: www.elsevier.com/locate/jpcs

# Unusual effect of high pressures on phase transformations in $Ni_{62}Nb_{38}$ alloy

Bulat N. Galimzyanov [a,b,*], Maria A. Doronina [a], Anatolii V. Mokshin [a,b]

[a] Kazan Federal University, 420008 Kazan, Russia
[b] Udmurt Federal Research Center of the Ural Branch of the Russian Academy of Sciences, 426067 Izhevsk, Russia

ARTICLE INFO

*Keywords:*
Phase diagram
Bulk metallic glass
Nickel alloys
Nanocrystalline materials
Molecular dynamics

ABSTRACT

Binary $Ni_{62}Nb_{38}$ alloy belongs to the unique class of binary off-eutectic systems, which are able to form a bulk glassy state (L. Xia et al., 2006). In the present work, the ($p$, $T$) phase diagram of $Ni_{62}Nb_{38}$ alloy was first determined for a wide thermodynamic range with temperatures from 300 K to 6000 K and with pressures from 1 atm to $1.2\times10^7$ atm. For this thermodynamic range, elements of the phase diagram such as the liquid–crystal coexistence line and the glass transition line are defined. Our results reveal good agreement between the simulation results and the known experimental values of the liquidus temperature and the glass transition temperature for the isobar $p = 1$ atm. The phase diagram is detailed for pressures greater than $1\times10^7$ atm. For the first time, the phase separation conditions at which the liquid Nb and crystalline Ni phases coexist in the system were determined.

Binary $Ni_{62}Nb_{38}$ alloy has a pronounced ability to form bulk metallic glass, which makes this alloy attractive for the manufacture of construction materials [1–5]. In the amorphous phase, this alloy has a hardness of approximately 15 GPa, a Young's modulus of approximately 230 GPa, and a fracture strength of approximately 4 GPa. Remarkably, the values of these mechanical characteristics are larger than for other binary bulk metallic glasses, including Ni-based ones [6–9]. $Ni_{62}Nb_{38}$ bulk metallic glass with a stable amorphous structure was synthesized at the beginning of the 21st century by traditional casting in copper molds [2]. It has been shown that off-eutectic $Ni_{62}Nb_{38}$ alloy is the best glass former in comparison with the Ni–Nb system with other ratios of components [10–12]. It is remarkable that this finding is not in agreement with the empirical rules, according to which bulk metallic glasses can be formed by a multicomponent alloy with a eutectic composition [13–16].

The structure and mechanical properties of $Ni_{62}Nb_{38}$ alloy depend on the thermodynamic ($p$, $T$) conditions in which the alloy is synthesized and/or used. Therefore, to determine properly the functional capabilities of this alloy, it is necessary to know the ($p$, $T$) ranges on the phase diagram at which the system can be in the liquid, crystalline, or glassy phase. Despite $Ni_{62}Nb_{38}$ alloy being used for the study of the mechanisms of formation of an amorphous structure [7,17,18], most studies consider this alloy only under standard conditions and in the thermodynamic states with pressures not greater than $1\times10^3$ atm. In addition, the liquidus line $T_l(p)$ and the glass transition line $T_g(p)$ were still unknown for this system. The dependencies $T_l(p)$ and $T_g(p)$ are difficult to determine experimentally because of problems with the realization of cooling and heating protocols at high pressures [19]. Therefore, there are still no experimental data to construct the detailed ($p$, $T$) phase diagram of binary $Ni_{62}Nb_{38}$ alloy. On the other hand, a comprehensive study of phase transformations in this system by molecular dynamics simulations became possible after the development of the modified Finnis–Sinclair interatomic interaction potential [20]. This semiempirical potential correctly reproduces the structure of this alloy in the liquid and amorphous states. This is confirmed by good agreement between the simulation results, quantum mechanical calculations, and the findings of X-ray diffraction experiments.

Phase separation in metal alloys into liquid and solid fractions can be observed at high pressures. For example, the phase separation into liquid and crystalline phases or into amorphous and crystalline phases has been observed in Al-based, Cu-based, and Ni-based binary and ternary alloys under high-pressure torsion [21,22]. For the off-eutectic compositions, the phase separation is known and it is a typical effect [23]. In the case of $Ni_{62}Nb_{38}$ alloy, the phase separation has not been observed previously.

The main aim of the present study is to determine such key elements of the ($p$, $T$) phase diagram of binary $Ni_{62}Nb_{38}$ alloy as the liquidus line $T_l = T_l(p)$ and the glass transition line $T_g = T_g(p)$ for a wide range of pressures. Similar studies have not been performed previously for this system. Knowledge of such information makes it possible to determine the crystalline phase region and the region where a bulk metallic glass

* Corresponding author at: Kazan Federal University, 420008 Kazan, Russia.
*E-mail addresses:* bulatgnmail@gmail.com (B.N. Galimzyanov), maria.doronina.0211@gmail.com (M.A. Doronina), anatolii.mokshin@mail.ru (A.V. Mokshin).

https://doi.org/10.1016/j.jpcs.2022.110995
Received 24 February 2022; Received in revised form 1 September 2022; Accepted 2 September 2022
Available online 6 September 2022

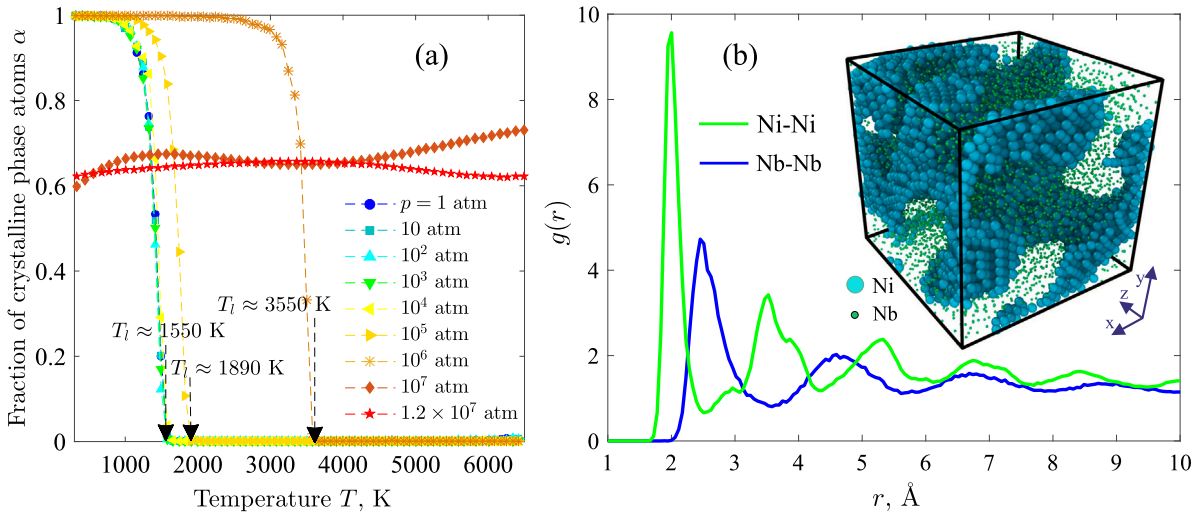


**Fig. 1.** (a) Temperature dependence of the fraction of crystalline phase atoms $\alpha$ for different isobars. Here $\alpha = n/N$, where $n$ is the number of atoms forming the crystalline phase and $N$ is the total number of atoms in the system. (b) Partial pair correlation function $g(r)$ for crystalline Ni and liquid Nb calculated at 6000 K and $1 \times 10^7$ atm. The inset shows a snapshot of the system, where Ni forms a branched crystalline structure, while Nb is in the liquid state.

is formed. We also solve the problem related to determining the ($p$, $T$) conditions at which the phase separation is observed.

In the current study, by means of molecular dynamics simulations we define the ($p$, $T$) phase diagram of binary $Ni_{62}Nb_{38}$ alloy covering the temperature range from 300 K to 6000 K and for pressures up to $1.2 \times 10^7$ atm. The main focus is on the estimation of the liquidus temperature $T_l$ and the glass transition temperature $T_g$ under various isobaric conditions. We consider the binary alloy with a fixed concentration of atoms: 7229 Ni atoms and 4435 Nb atoms are located inside the simulation cubic box with edge length $L \approx 63.3$ Å. The integration of the equations of motion is performed with a time step of 1 fs. Temperature and pressure are controlled by a thermostat and a barostat according to the Nose–Hoover method [24]. The interatomic energies and forces are determined by the semiempirical Finnis–Sinclair potential adapted by Mendelev to reproduce properly the structure and dynamic properties of Ni–Nb alloys in liquid and solid phases [20]. Molecular dynamics simulations were performed with the LAMMPS package [25]. Identification of crystalline structures, pair correlation analysis, and visualization of the simulation results were done with the program OVITO [26].

The crystalline samples were heated to 6000 K at the rate $1 \times 10^{11}$ K/s. This fast heating rate is acceptable for molecular dynamics simulations and does not introduce undesirable artifacts such as excessive overlap of atoms, drift of atoms outside the simulation cell, and incorrect control of temperature and pressure [20,27]. The liquidus points on the isobars were determined from the temperature dependencies of the crystalline phase fractions $\alpha$. Fig. 1(a) shows the temperature dependencies of $\alpha$ for various isobars. The liquidus point corresponds to the temperature $T_l$ at which the system does not contain any crystalline domains and $\alpha$ becomes 0. We found that the liquidus temperature $T_l \simeq (1550 \pm 20)$ K at 1 atm, which is in excellent agreement with the experimental value $T_l^{(Exp)} \simeq 1543$ K [28]. In the pressure range from 1 atm to $1 \times 10^3$ atm, the liquidus temperature increases by only 50 K (up to approximately 1600 K), which is comparable to the statistical error. A significant increase in the liquidus temperature from approximately 1650 K to approximately 3550 K is observed at pressures from $1 \times 10^4$ atm to $1 \times 10^6$ atm [see Fig. 1(a)]. For pressures greater than $1 \times 10^6$ atm, the liquidus temperature goes beyond the considered temperature range. The value of the parameter $\alpha(T)$ fluctuates in the range from 0.6 to 0.8 at pressures $1 \times 10^7$ atm and $1.2 \times 10^7$ atm because of the coexistence of solid and liquid phases.

The partial pair correlation function $g(r)$ was computed for the system at 6000 K and $1 \times 10^7$ atm. As can be seen from Fig. 1(b), $g(r)$ computed for Ni–Ni and Nb–Nb has features that can be considered as signatures of the so-called phase separation: Ni is in the crystalline phase, while Nb is in the liquid state. The phase separation is directly detected in a snapshot [inset in Fig. 1(b)], where crystalline Ni domains are embedded in liquid Nb. As we showed earlier [29], such a redistribution of Ni and Nb atoms is the result of an applied pressure, and not the result of heating.

Fig. 2(a) shows the fraction of the crystalline Ni atoms forming the hexagonal close packed (hcp), face-centered cubic (fcc), and body-centered cubic (bcc) phases at $1 \times 10^7$ atm and in the temperature range from 300 K to 6000 K. The results indicate the predominance of the hcp phase, while the fraction of the fcc and bcc phase atoms is comparable and does not exceed 40%. It is noteworthy that Ni appears in the hcp and fcc modifications as in the case of pure Ni [30]. Crystalline Ni also appears as an unstable bcc phase. These results agree with the literature data. It was shown earlier in experimental and simulation studies that Ni can exist in the hcp and fcc phases and in the unstable bcc phase at pressures above 100 GPa [31–34]. Structural rearrangements between the fcc, hcp, and bcc phases are possible at such extremely high pressures, which can occur in solids at terapascal pressures [35,36]. In Fig. 2(b), calculated $g(r)$ reveals structural changes in Nb under the considered ($p$, $T$) conditions. We found that Nb is in the amorphous state at $1 \times 10^7$ atm and 300 K. This is confirmed by the presence of the pronounced first maximum and the characteristic splitting of the second maximum of $g(r)$. The amorphous structure is destroyed with increasing temperature, and Nb completely transforms into a liquid state at approximately 4800 K. It is remarkable that the similar phase separation in a binary metallic system, at which the liquid/glassy phase of one component and the crystalline phase of other component coexist, has not been observed before at pressures greater than $1 \times 10^7$ atm. In this regard, such separation in $Ni_{62}Nb_{38}$ is an unusual effect. In addition, this effect is unusual in that a similar phase separation in binary and ternary metallic systems based on Fe, Al, Cu, and Ni was previously found only for steady-state non-equilibrium conditions when the system is under a moderate pressure (less than $1 \times 10^4$ atm) and torsion load [21,22,37–40]. For example, the phase separation under compression and heating were observed earlier in experimental and simulation studies of binary Fe–Cr [41], Fe–Cu [42], and Cu–Co [43] alloys as well as multicomponent Fe–Cu–Ge [44] and $LiFePO_4$ [45] alloys. Pressure-induced amorphization is most often found in various rocks and minerals formed in the earth entrails [46]. Therefore, the predicted impact of pressure on the phase separation in $Ni_{62}Nb_{38}$ alloy seems to be correct.

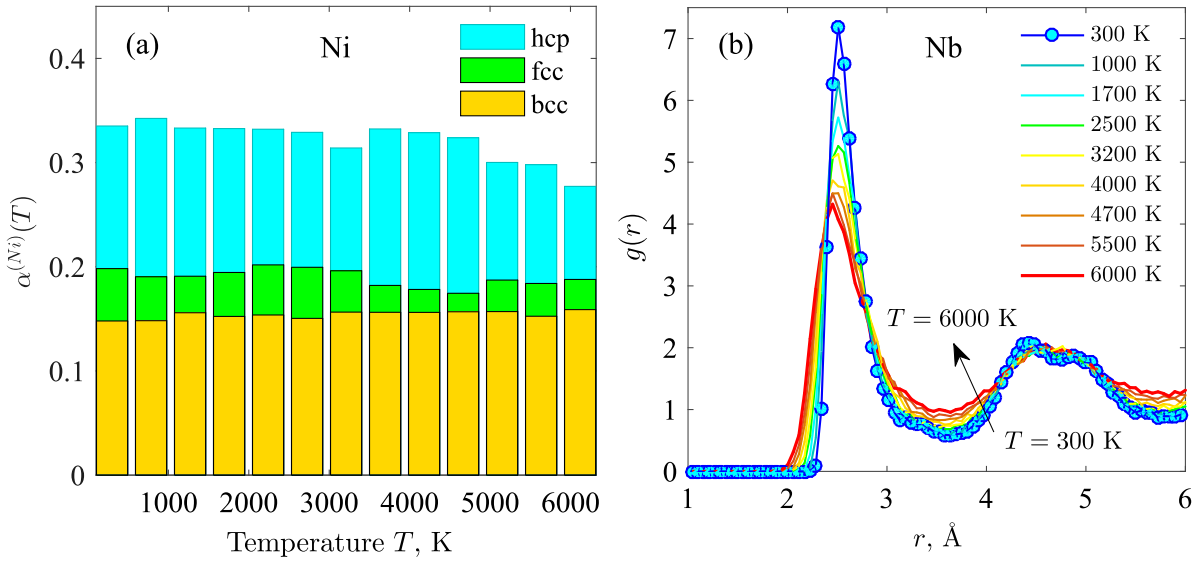


**Fig. 2.** (a) Fraction of Ni atoms in hexagonal close packed (hcp), face-centered cubic (fcc), and body-centered cubic (bcc) crystalline phases as a function of the temperature $T$ at $1 \times 10^7$ atm. (b) Pair correlation function for Nb at various temperatures. This figure shows the transition from the amorphous state to the liquid state that occurs when the system is heated from 300 K to 6000 K at $1 \times 10^7$ atm.

**Table 1**
System parameters at different pressures $p$: $T_l$ is the liquidus temperature, $T_g$ is the glass transition temperature.

| $p$, atm | $T_l$, K | $T_g$, K |
|---|---|---|
| 1 | $1550 \pm 20$ | $1020 \pm 50$ |
| 10 | $1560 \pm 20$ | $1030 \pm 50$ |
| $1 \times 10^2$ | $1575 \pm 20$ | $1050 \pm 60$ |
| $1 \times 10^3$ | $1600 \pm 25$ | $1080 \pm 60$ |
| $1 \times 10^4$ | $1650 \pm 25$ | $1130 \pm 60$ |
| $1 \times 10^5$ | $1890 \pm 30$ | $1220 \pm 70$ |
| $1 \times 10^6$ | $3550 \pm 50$ | $1780 \pm 80$ |

The glass transition conditions were determined during rapid cooling of equilibrium liquid melt. A liquid system with temperature $1.5T_l$ was cooled at the rate $1 \times 10^{12}$ K/s to 300 K on various isobars. The glass transition temperature $T_g$ is determined from the change in the difference between the potential energy $E$ and the kinetic energy $3k_BT$ at decreasing temperature $T$. Fig. 3(a) shows the temperature dependence of the difference $E - 3k_BT$ computed at different pressures. It can be seen from Fig. 3(a) that these dependencies contain two regimes: (i) the high-temperature regime, corresponding to the liquid state, in which the energy decreases rapidly; and (ii) the low-temperature regime, corresponding to the frozen state, where the energy decreases slowly. The boundary between these regimes on the temperature scale directly corresponds to the glass transition temperature $T_g$ [see Fig. 3(a)]. The size of this boundary determines the error interval in the found values of $T_g$ (see Table 1).

In Fig. 3(b), the computed structure factor $S(k)$ of amorphous $Ni_{62}Nb_{38}$ alloy is compared with the X-ray diffraction data [20,47]. The simulation data and the experimental data were obtained under identical thermodynamic conditions. As can be seen from Fig. 3(b), there is excellent agreement between the simulation data and the X-ray diffraction data except in the region of wave numbers corresponding to the second peak of the static structure factor $S(k)$. Further, the glass transition temperature $T_g \simeq 1020$ K at 1 atm is close to the known experimental value $T_g^{(Exp)} = 891$ K [47]. As is known, the faster the cooling rate, the greater the glass transition temperature $T_g$ [48,49]. In the present work, the cooling rate is $1 \times 10^{12}$ K/s, while in Ref. [47] the reported results were obtained for the case of cooling at a rate of approximately 10 K/s. Therefore, it is quite obvious that the obtained glass transition temperature is approximately 130 K larger than the experimental glass transition temperature.

Fig. 4 shows the ($p$, $T$) phase diagram obtained for $Ni_{62}Nb_{38}$ alloy. In this diagram, the liquid–solid equilibrium lines and the boundaries of the phase separation regions are depicted. We found that the pressure dependence of the calculated liquidus temperature $T_l$ is accurately reproduced by the well-known Simon–Glatzel (SG) empirical equation [50,51]:

$$T_l(p) = T_{l0}\,(1 + \beta p)^{\xi}\,. \tag{1}$$

This equation has a simple form and contains a minimum number of adjustable parameters compared with other empirical equations and its modifications. In Eq. (1), $T_{l0} \simeq 1550$ K is the liquidus temperature at $p = 1$ atm. The adjustable quantities $\beta$ and $\xi$ are related to the Grüneisen parameter [50]. The best agreement between the simulation data and Eq. (1) was obtained with $\beta \simeq (7.5 \pm 2.0) \times 10^{-6}$ atm$^{-1}$ and $\xi \simeq 0.38 \pm 0.4$. These values are comparable with known literature data obtained for metals. For example, the melting line of pure nickel is reproduced by Eq. (1) with $\beta \simeq 1 \times 10^{-6}$ atm$^{-1}$ and $\xi \simeq 0.45$ (see Table I in Ref. [52]), which are close to the found values for $Ni_{62}Nb_{38}$ alloy.

As can be seen from Fig. 4, the correspondence between the temperature $T$ and the pressure $p$ for the glass transition is similar to the liquidus line. Therefore, it is also convenient to interpolate the data obtained for the glass transition by the SG-type equation [50,53]

$$T_g(p) = T_{g0}\left(1 + \frac{p}{\Pi}\right)^{1/b}. \tag{2}$$

Note that Eq. (2) is identical to the phenomenological Andersson–Andersson equation [54]. Here, $T_{g0} \simeq 1020$ K is the glass transition temperature at $p = 1$ atm. $\Pi$ and $b$ are adjustable and depend on the system type. $\Pi$ has the dimension of pressure, while the dimensionless parameter $b$ is defined through the volume expansion coefficient and the specific heat capacity of the system [53]. For the binary alloy considered, we found that $\Pi \simeq (33 \pm 10) \times 10^3$ atm and $b \simeq 6.25 \pm 1.0$. The $T_g(p)$ dependence obtained for $Ni_{62}Nb_{38}$ alloy by Eq. (2) is correct and similar in shape to the experimentally measured glass transition lines of real glass-forming systems [55,56]. Note that the obtained dependencies $T_l(p)$ and $T_g(p)$ are in agreement with previous results [50,55]. Namely, the found values of the exponents in SG-type Eqs. (1) and (2) belong to the interval (0; 1), which is valid for various types of liquid (including metallic ones) with pronounced glass-forming ability [52].

In summary, the ($p$, $T$) phase diagram of $Ni_{62}Nb_{38}$ alloy was first determined for a wide thermodynamic range. The liquidus temperature

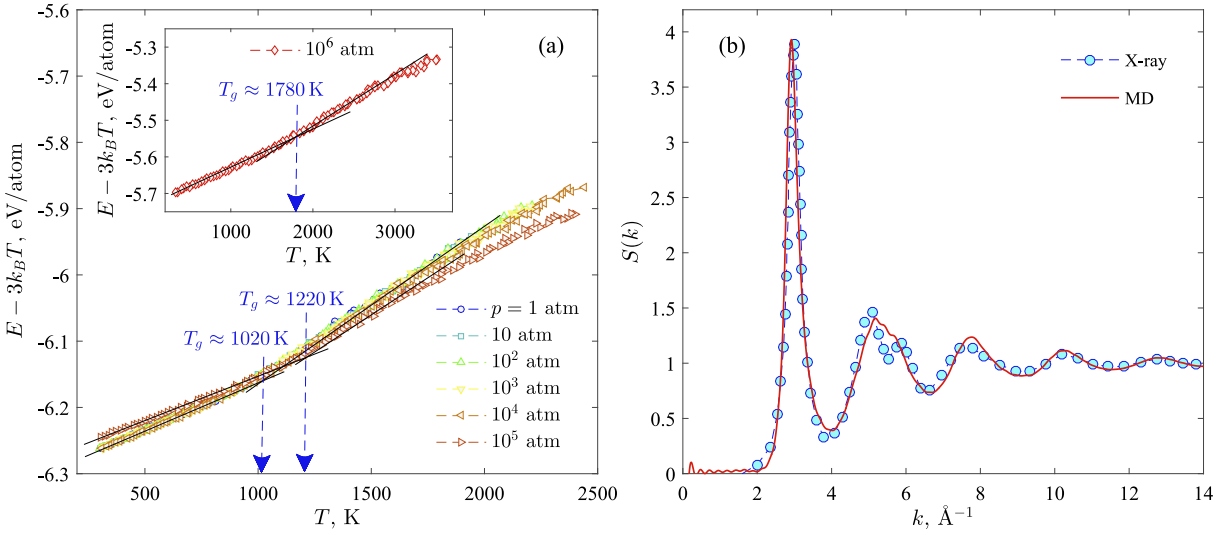


**Fig. 3.** (a) Difference $E - 3k_BT$ between potential and kinetic energies of the system as a function of the temperature $T$ at different isobars. (b) Structure factor $S(k)$ calculated through molecular dynamics simulations (MD) at 300 K and 1 atm compared with X-ray diffraction data [20,47].

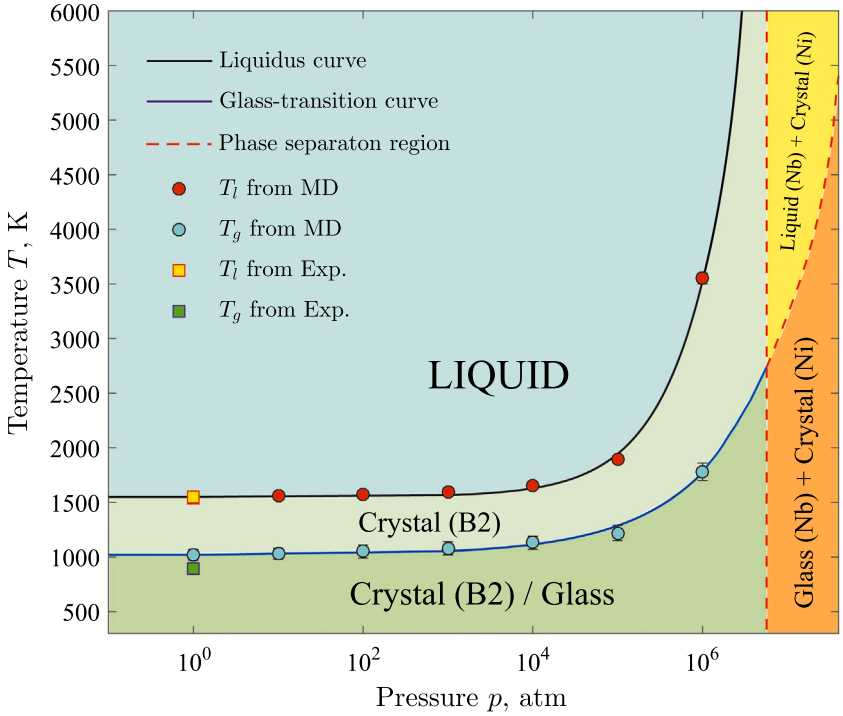


**Fig. 4.** ($p$, $T$) phase diagram of $Ni_{62}Nb_{38}$ alloy. The pressure is presented on a logarithmic scale. The liquidus line (black) and the glass transition line (blue) were obtained with use of Eqs. (1) and (2), respectively. The circles indicate the calculated temperatures $T_l$ and $T_g$ taken from Table 1. The squares denote the experimentally measured temperatures $T_l$ and $T_g$ at 1 atm [28,47]. The dotted red lines indicate the phase separation regions at pressures $p \geq 1 \times 10^7$ atm. Exp., experiments; MD, molecular dynamics simulations.

$T_l$ and the glass transition temperature $T_g$ as a function of the pressure $p$ were determined. We have shown that obtained dependencies $T_l(p)$ and $T_g(p)$ are reproduced by the well-known SG-type empirical equations. The phase separation is observed at pressures above $1 \times 10^7$ atm: Nb is in the liquid state, while Ni forms a percolating crystal structure. This result is of great fundamental importance since it shows that the pressure is one of the main thermodynamic parameters that allows one to control the phase transformations in $Ni_{62}Nb_{38}$ alloy. Therefore, the results of the present work could be a starting point for study of the thermodynamics of Ni–Nb systems with various concentrations of Ni atoms.

## Funding

This work was supported by the Russian Science Foundation (project no. 19-12-00022-P). MAD and AVM acknowledge the Theoretical Physics and Mathematics Advancement Foundation "BASIS" (No. 20-1-2-38-1) for supporting the computational part of this work.

## CRediT authorship contribution statement

**Bulat N. Galimzyanov:** Methodology, Investigation, Formal analysis, Writing – original draft. **Maria A. Doronina:** Software, Methodology, Investigation. **Anatolii V. Mokshin:** Conceptualization, Writing – review & editing.

## Declaration of competing interest

The authors declare that they have no known competing financial interests or personal relationships that could have appeared to influence the work reported in this paper.

## Data availability

No data was used for the research described in the article.

## Appendix A. Supplementary material

Supplementary material related to this article can be found online at https://doi.org/10.1016/j.jpcs.2022.110995.

## References


[1] M.R. Jones, F.W. DelRio, J.W. Pegues, P. Lu, R. Puckett, N.S. Bobbitt, T.J. Hardin, M. Chandross, A.B. Kustas, N. Argibay, J. Mater. Res. 36 (2021) 3167–3181.
[2] L. Xia, W.H. Li, S.S. Fang, B.C. Wei, Y.D. Dong, J. Appl. Phys. 99 (2006) 026103.
[3] A.V. Maiorova, T.V. Kulikova, R.E. Ryltsev, Phil. Mag. 101 (2021) 1709–1725.
[4] J. Jeon, G. Kim, N. Seo, H. Choi, H.-J. Kim, M.-H. Lee, H.-K. Lim, S.B. Son, S.-J. Lee, J. Mater. Res. Technol. 16 (2022) 129–138.
[5] B.A. Klumov, R.E. Ryltsev, N.M. Chtchelkatchev, J. Chem. Phys. 149 (2018) 134501.
[6] W. Lu, J.-C. Tseng, A. Feng, J. Shen, J. Non-Cryst. Solids 564 (2021) 120834.
[7] L. Xia, S.T. Shan, D. Ding, Y.D. Dong, Intermetallics 15 (2007) 1046–1049.
[8] B.N. Galimzyanov, A.V. Mokshin, Int. J. Solids Struct. 224 (2021) 111047.
[9] R.M. Khusnutdinoff, R.R. Khairullina, A.L. Beltyukov, V.I. Lad'yanov, A.V. Mokshin, J. Phys. Condens. Matter 33 (2021) 104006.
[10] Q. Cheng, P.F. Wang, H.Y. Jiang, L. Gu, J. Orava, Y.H. Sun, H.Y. Bai, W.H. Wang, Phys. Rev. B 103 (2021) L100203.
[11] Y.Q. Zeng, J.S. Yu, Y. Tian, A. Hirata, T. Fujita, X.H. Zhang, N. Nishiyama, H. Kato, J.Q. Jiang, A. Inoue, M.W. Chen, Acta Mater. 200 (2020) 710–719.
[12] B.N. Galimzyanov, V.I. Ladyanov, A.V. Mokshin, J. Cryst. Growth 526 (2019) 125214.
[13] A.V. Mokshin, B.N. Galimzyanov, D.T. Yarullin, Eur. Phys. J. Spec. Top. 229 (2020) 427–432.
[14] D.V. Alexandrov, P.K. Galenko, I.O. Starodumov, Eur. Phys. J. Spec. Top. 229 (2020) 141–143.
[15] M. Baggioli, A. Zaccone, Internat. J. Modern Phys. B 35 (2021) 2130002.
[16] N.K. Ngan, A.D. Phan, A. Zaccone, Rapid Res. Lett. 15 (2021) 2100235.
[17] T. Wen, Y. Zhang, C. Wang, N. Wang, K. Ho, M. Kramer, Intermetallics 98 (2018) 131–138.
[18] M. Manna, S. Pal, Mater. Sci. Forum 978 (2020) 436–445.
[19] J.Y. Zhang, Z.Q. Zhou, Z.B. Zhang, M.H. Park, Q. Yu, Z. Li, J. Ma, A.D. Wang, H.G. Huang, M. Song, B.S. Guo, Q. Wang, Y. Yang, Mater. Futures 1 (2022) 012001.
[20] Y. Zhang, R. Ashcraft, M.I. Mendelev, C.Z. Wang, K.F. Kelton, J. Chem. Phys. 145 (2016) 204505.
[21] Á. Révész, S. Hóbor, J.L. Lábár, A.P. Zhilyaev, Zs Kovácz, J. Appl. Phys. 100 (2006) 103522.
[22] B. Straumal, A. Korneva, P. Zieba, Arch. Civ. Mech. Eng. 14 (2014) 242–249.
[23] H. Okamoto, J. Phase Equilibria Diffus. 29 (2008) 210.
[24] J.M. Thijssen, Computational Physics, second ed., Cambridge University Press, 2007.
[25] S. Plimpton, J. Comput. Phys. 117 (1995) 1–19.
[26] A. Stukowski, Model. Simul. Mater. Sci. Eng. 18 (2009) 015012.
[27] M.I. Mendelev, M.J. Kramer, J. Appl. Phys. 107 (2010) 073505.
[28] S. Lesz, G. Dercz, J. Therm. Anal. Calorim. 126 (2016) 19–26.
[29] B.N. Galimzyanov, M.A. Doronina, A.V. Mokshin, J. Non-Cryst. Solids 572 (2021) 121102.
[30] P. Li, P. Zhang, F. Li, W. Jiang, Z. Cao, J. Sol.-Gel. Sci. Technol. 68 (2013) 261–269.
[31] S. Boccato, R. Torchio, I. Kantor, G. Morard, S. Anzellini, R. Giampaoli, R. Briggs, A. Smareglia, T. Irifune, S. Pascarelli, J. Geophys. Res. Solid Earth 122 (2017) 9921–9930.
[32] L. Dubrovinsky, N. Dubrovinskaia, O. Narygina, I. Kantor, A. Kuznetzov, V.B. Prakapenka, L. Vitos, B. Johansson, A.S. Mikhaylushkin, S.L. Simak, I.A. Abrikosov, Science 316 (2007) 1880–1883.
[33] S. Tateno, K. Hirose, T. Komabayashi, H. Ozawa, Y. Ohishi, Geophys. Res. Lett. 39 (2012) L12305.
[34] E.G.C. Neiva, M.M. Oliveira, L.H. Marcolino, A.J.G. Zarbin, J. Colloid Interface Sci. 468 (2016) 34–41.
[35] L. Dubrovinsky, S. Khandarkhaeva, T. Fedotenko, et al., Nature 605 (2022) 274–278.
[36] C. Pickard, R. Needs, Nature Mater. 9 (2010) 624–627.
[37] W.H. Wang, R.J. Wang, D.Y. Dai, D.Q. Zhao, M.X. Pan, Y.S. Yao, Appl. Phys. Lett. 79 (2001) 1106–1108.
[38] X.R. Liu, S.M. Hong, S.J. Lü, R. Shen, Appl. Phys. Lett. 91 (2007) 081910.
[39] A.S. Poryvaev, D.M. Polyukhov, M.V. Fedin, ACS Appl. Mater. Interfaces 12 (2020) 16655–16661.
[40] D.T. Yarullin, B.N. Galimzyanov, A.V. Mokshin, J. Chem. Phys. 152 (2020) 224501.
[41] J. Zhou, J. Odqvist, M. Thuvander, P. Hedström, Microsc. Microanal. 19 (2013) 665–675.
[42] Y. Cheng, W. Cui, L. Wang, C. Peng, S. Wang, Y. Wang, Metals 7 (2017) 73.
[43] A. Bachmaier, M. Pfaff, M. Stolpe, H. Aboulfadl, C. Motz, Acta Mater. 96 (2015) 269–283.
[44] S.B. Luo, W.L. Wang, Z.C. Xia, B. Wei, J. Alloy. Compd. 717 (2017) 190–196.
[45] K. Yang, M. Tang, J. Mater. Chem. A 8 (2020) 3060–3070.
[46] P. Richet, P. Gillet, Eur. J. Mineral. 9 (1997) 907–934.
[47] N.A. Mauro, M.L. Johnson, J.C. Bendert, K.F. Kelton, J. Non-Cryst. Solids 362 (2013) 237–245.
[48] A.S. Ninarello, Computer Simulations of Supercooled Liquids Near the Experimental Glass Transition (Doctoral thesis), University of Montpellier, 2017.
[49] J.M. Hutchinson, J. Therm. Anal. Calorim. 98 (2009) 579–589.
[50] H. Schlosser, P. Vinet, J. Ferrante, Phys. Rev. B 40 (1989) 5929–5935.
[51] D. Errandonea, J. Appl. Phys. 108 (2010) 033517.
[52] S.E. Babb, Rev. Modern Phys. 35 (1963) 400–413.
[53] K. Kaminski, S. Pawlus, K. Adrjanowicz, Z. Wojnarowska, P. Wlodarczyk, M. Paluch, J. Phys. Condens. Matter 24 (2012) 065105.
[54] S.P. Andersson, O. Andersson, Macromolecules 31 (1998) 2999–3006.
[55] A. Drozd-Rzoska, S.J. Rzoska, A.R. Imre, J. Non-Cryst. Solids 353 (2007) 3915–3923.
[56] J. Buchholz, W. Paul, F. Varnik, K. Binder, J. Chem. Phys. 117 (2002) 7364–7372.